7330 *Inorg. Chem.* **2009**, *48*, 7330–7340
DOI: 10.1021/ic9008202

Inorganic Chemistry
Article

Heteronuclear and Homonuclear Cu^{2+} and Zn^{2+} Complexes with Multihistidine Peptides Based on Zebrafish Prion-like Protein

Daniela Valensin,*,† Łukasz Szyrwiel,‡ Francesca Camponeschi,† Magdalena Rowińska-Żyrek,‡ Elena Molteni,† Elzbieta Jankowska,§ Aneta Szymanska,§ Elena Gaggelli,† Gianni Valensin,† and Henryk Kozłowski*,‡

†*Department of Chemistry, University of Siena, Via Aldo Moro, 53100 Siena, Italy,* ‡*Faculty of Chemistry, University of Wrocław, F. Joliot-Curie 14, 50-383 Wrocław, Poland, and* §*Faculty of Chemistry, University of Gdańsk, 80-952 Gdańsk, Poland*

Received April 28, 2009

The homeostasis of metal ions, especially copper and zinc, is a major factor that may influence the prion diseases and the biological function of prion protein (PrP). The His-rich regions are basic sites for metal binding and antioxidant activity of the PrP structures. Animal prion-like proteins contain also His-rich domains, and their coordination chemistry may provide better insight into the chemistry and biology of PrP structures and related diseases. Herein, we report an equilibrium study on heteronuclear $Zn^{2+}-Cu^{2+}$ complexes with zrel-PrP fragments from zebrafish. Potentiometric, spectroscopic, and mass spectrometric methods showed that the binding of copper is much more effective than the binding of zinc. At physiological pH, both metals bind to the histidine imidazole N donors of the studied peptides.

Introduction

The prion protein (PrP) is a membrane glycoprotein found mostly in neurons.[1] In its structure, two domains can be distinguished:[2,3] a globular structured C-terminal domain and an N-terminal flexible domain composed of about 100 amino acids. This N-terminal domain is well conserved in all species, and it contains a histidine-rich region that interacts with metal ions.[4,5] The physiological role of PrP is still unknown. However, it is clear that it binds copper ions in vivo[6] and it seems to play two basic biological functions:

(i) The transport of Cu^{2+} ions and perhaps Zn^{2+}. In vivo it has been observed that when PrP is exposed to metal ions like copper or zinc, the process of internalization of the protein into the cell takes place.[5,7]

(ii) Antioxidant function (SOD-like activity). Cu^{2+} ions bound to PrP are able to decrease the level of reactive oxygen species, mimicking the activity of copper−zinc superoxide dismutase (CuZn-SOD), an enzyme whose active center contains a heteronuclear Cu−Zn cluster bridged by an imidazole ring of a histidyl residue.[8]

It has been shown[9,10] that one of the most likely functions of PrP^C in the presynaptic space is SOD-like activity. This function is abolished either when the octarepeat region involved in the copper ion binding is removed or when a copper chelator (for example, diethyldithiocarbamate) is added.[11] The SOD-like activity was reported for both mouse and chicken full-length recombinant PrP structures, which were refolded in the presence of copper.[11]

The change of the native structure of PrP (PrP^C) into the insoluble and protease-resistant form (PrP^{Sc}) leads to fatal neurodegenerative disorders like Kuru and Creutzfeld-Jacob diseases in human and spongiform encephalopathies in cattle and sheep. The reason of these neurodegenerative disorders is not yet well understood.[12] Metal ions can play a critical role in the development of these diseases.[13]

The interaction of copper with PrP in the His-rich region has been proven in both in vitro and in vivo experiments.[5] The imidazole ring of His is the basic anchoring group for copper ions in vivo.[14] In the human protein, the His groups are

*To whom correspondence should be addressed. E-mail: valensindan@unisi.it (D.V.), henrykoz@wchuwr.pl (H.K.).

(1) Boston, M.; McKinley, P.; Prusiner, S. B. *Science* **1982**, *218*, 1309–1311.
(2) Donne, D. G.; Viles, J. H.; Groth, D.; Mehlhorn, I.; James, T. L.; Cohen, F. E.; Prusiner, S. B.; Wright, P. E.; Dyson, H. J. *Proc. Natl. Acad. Sci. U.S.A.* **1997**, *94*, 13452-7.
(3) Riek, R.; Hornemann, S.; Wider, G.; Glockshuber, R.; Wüthrich, K. *FEBS Lett.* **1997**, *413*, 282–288.
(4) Sigel, A.; Sigel, H.; Sigel, R. K. O. *Metal Ions in Life Sciences*; Wiley: New York, 2008; Vol. *1*.
(5) Kozlowski, H.; Brown, D. R.; Valensin, G. *Metallochemistry of Neurodegeneration*; RSC Publishing: Cambridge, U.K., 2006.
(6) Brown, D. R.; Qin, K.; Herms, J. W.; Madlung, A.; Manson, J.; Strome, R.; Fraser, P. E.; Kruck, T. A.; Bohlen, A.; Schulz-Schaeffer, W.; Giese, A.; Westaway, D.; Kretzschmar, H. A. *Nature* **1997**, *390*, 684–687.
(7) Sumudhu, W.; Perera, S.; Hooper, N. M. *Curr. Biol.* **2001**, *11*, 519–523.
(8) Tainer, J. A.; Getzoff, E. D.; Beem, K. M.; Richardson, J. S.; Richardson, D. C. *J. Mol. Biol.* **1982**, *160*, 181–217.
(9) Brown, D. R.; Besinger, A. *Biochemistry* **1998**, *334*, 423–429.
(10) Brown, D. R.; Clive, C.; Haswell, S. J. *J. Neurochem.* **2001**, *76*, 69–76.
(11) Brown, D. R.; Wong, B. S.; Hafiz, F.; Clive, C.; Haswell, S. J.; Jones, I. M. *Biochem. J.* **1999**, *344*, 1–5.
(12) Prusiner, S. B. *Proc. Natl. Acad. Sci. U.S.A.* **1998**, *95*, 13363–13383.
(13) Choi, C. J.; Kanthasamy, A.; Anantharam, V.; Kanthasamy, A. G. *Neurotoxicology* **2006**, *5*, 777–787.
(14) Łuczkowski, M.; Kozłowski, H.; Łęgowska, A.; Rolka, K.; Remelli, M. *J. Chem. Soc., Dalton Trans.* **2003**, 619–624.

 Published on Web 07/08/2009

separated by seven amino acids without any effective metal binding group between them. The structure of this fragment makes it a very effective binding unit for Cu^{2+} because of the set of His imidazoles[15] but rather not effective for Zn^{2+} because the His residues are too far from each other.

Mammalian neurons are not the only ones that contain PrP structures. Prion-like proteins are also present in lower species like birds and fishes.[16,17] In all of these species, we can distinguish a His-rich repeat region. In avian PrP structures, His groups are separated by five amino acids, while in fishes, these repeats are less regular and His residues are even closer to each other.[15] It was shown that duplication of zebrafish rel-PrP genes yields two proteins: PrP-rel-1 (zebrafish PrP3) and Prp-rel-2 (zebrafish-like PrP).[18,19] In the biogenesis of mammalian PrP^C, two phases of post-translational modifications can be characterized (reviewed in refs 20 and 21): (i) modification with two N-linked glycans after the import into the endoplasmic ER and (ii) formation of a disulfide bridge and a glycosylphosphatidylinositol (GPI) anchor at serine 230.[22] Finally, the PrP^C remains bound to the plasma membrane. The biogenesis of zebrafish-like PrP seems to be very similar. The import of the protein into the ER and the modification with glycans were observed. This protein is also a GPI-anchored cell surface protein. The Prp-rel-2 region encompassing residues 60−87 contains effective metal binding sites similar to regions found in fugu StPrP, and the efficiency of Cu^{2+} binding is comparable or even better than that of mammalian PrP^C fragments.[15,23] The concentration of Zn^{2+} in the PrP environment is at least 4 times larger than the concentration of copper.[23,24] The 5−15% of the zinc fraction in the brain exists at millimolar concentrations.[25] Both Zn^{2+} and Cu^{2+} ions can trigger the endocytosis of PrP in humans.[26,27] Zinc binding to human PrP was recently investigated, and the effects of Zn^{2+} on Cu^{2+} coordination were discussed.[28] Two different mechanisms of action were suggested: a direct zinc binding to the octarepeat region or a shift in the copper binding mode indirectly induced by Zn^{2+}. Moreover, it was shown that fish-like PrP structures are very effective ligands for both Cu^{2+} and Zn^{2+} ions.[29−31] The fish protein contains His groups separated by only two amino acid residues, which makes them effective binding sites for Zn^{2+}. The fact that Zn^{2+} favors binding to imidazoles, which are in close proximity, is well described in the literature.[32,33] Additionally, the presence of polyhistidine sequences can cause a cooperative effect in the binding of Zn^{2+}. Many studies show that His-rich peptides effectively bind Cu^{2+} [34] and Zn^{2+} [35,36] in homo- and heteronuclear complexes.[37]

In the past decade, the SOD-like activity of Cu^{2+}−peptide complexes[38,39] and the SOD-like activity of both human and avian PrP peptide fragments with Cu^{2+} have been reported.[30,40]

In the native SOD, the catalytic Cu^{2+} ion is coordinated by three imidazole rings and a water molecule, while the structural Zn^{2+} is bound to two imidazoles and a carboxyl group of an aspartyl residue. The two metal ions are bridged by an additional imidazole residue of His-61, whose Nδ and Nε atoms fill the remaining coordination sites of the metal ions. This results in a five-coordinated distorted octahedral geometry for Cu^{2+} and a distorted tetrahedron for Zn^{2+}.

Cu^{2+} is crucial for the catalytic SOD activity, while the roles of the imidazolate bridge and Zn^{2+} are less well understood and seem to play a different role rather than a catalytic one.

The aim of this study was to investigate simultaneous copper and zinc binding to the zebrafish PrP-rel protein. The formation of heteronuclear species was proved by electrospray ionization mass spectrometry (ESI-MS) techniques, while NMR, circular dichroism (CD), and potentiometry allowed characterization of the Zn−Cu complexes. In order to better understand the chemical features of these species, a further analysis of the homonuclear copper and zinc complexes was also necessary. Three different protein fragments encompassing residues 63−87 were analyzed, and all of the experimental evidence was used to build up structural models used for molecular dynamics calculations. In addition, the SOD-like activity of the systems containing Cu^{2+} and both Cu^{2+} and Zn^{2+} complexes was measured by using an indirect method.

Materials and Methods

Potentiometric Measurements. All data were calculated from three titrations carried out over the pH range 2.5−10.5 at 25 °C

(15) Kozłowski, H.; Janicka-Kłos, A.; Stańczak, P.; Valensin, D.; Valensin, G.; Kulon, K. *Coord. Chem. Rev.* **2008**, *252*, 1069–1078.
(16) Harris, D. A.; Falls, D. L.; Frances, F. A.; Johnson, A.; Fischbach, G. D. *Proc. Natl. Acad. Sci. U.S.A.* **1991**, *88*, 7664–7668.
(17) Simonic, T.; Duga, S.; Strumbo, B.; Asselta, R.; Ceciliani, F.; Ronchi, S. *FEBS Lett.* **2002**, *469*, 33–38.
(18) Rivera-Milla, E.; Oidtmann, B.; Panagiotidis, C. H.; Baier, M.; Sklaviadis, T.; Hoffmann, R.; Zhou, Y.; Solis, G. P.; Stuermer, C. A. O.; Malaga-Trillo, E. *J. FASEB* **2005**, *2*, 317–336.
(19) Suzuki, T.; Kurokawa, T.; Hashimoto, H.; Sugiyama, M. *Biochem. Biophys. Res. Commun.* **2002**, *294*, 912–917.
(20) Tatzelt, J.; Winklhofer, K. F. *Amyloid* **2004**, *11*, 162–172.
(21) Miesbauer, M.; Bamme, T.; Riemer, C.; Oidtmann, B.; Winklhofer, K. F.; Baier, M.; Tatzelt, J. *Biochem. Biophys. Res. Commun.* **2006**, *341*, 218–224.
(22) Haraguchi, T.; Fisher, S.; Olofsson, S.; Endo, T.; Groth, D.; Tarentino, A.; Borchelt, D. R.; Teplow, D.; Hood, L.; Burlingame, A.; Lycke, E.; Kobata, A.; Prusiner, S. B. *Arch. Biochem. Biophys.* **1989**, *274*, 1–13.
(23) Leach, S. P.; Salman, M. D.; Hamar, D. *Animal Health Res. Rev.* **2006**, *7*, 97–105.
(24) Takeda, A. *Brain Res. Brain Res. Rev.* **2000**, *34*, 137–148.
(25) Frederickson, C. J. *Int. Rev. Neurobiol.* **1989**, *31*, 145–238.
(26) Sumudhu, W.; Perera, S.; Hooper, N. M. *Curr. Biol.* **2001**, *7*, 519–523.
(27) Brown, L. R.; Harris, D. A. *J. Neurochem.* **2003**, *87*, 353–363.
(28) Walter, E. D.; Stevens, D. J.; Visconte, M. P.; Millhauser, G. L. *J. Am. Chem. Soc.* **2007**, *129*(50), 15440–15441.
(29) Gaggelli, E.; Jankowska, E.; Kozlowski, H.; Marcinkowska, A.; Migliorini, C.; Stanczak, P.; Valensin, D.; Valensin, G. *J. Phys. Chem. B* **2008**, *47*, 15140–15150.
(30) Stańczak, P.; Kozłowski, H. *Biochem. Biophys. Res. Commun.* **2007**, *352*, 198–202.
(31) Szyrwiel, Ł.; Jankowska, E.; Janicka-Kłos, A.; Szewczuk, Z.; Valensin, D.; Kozłowski, H. *Dalton Trans.* **2008**, 6117–6120.
(32) Kallay, C.; Osz, K.; David, A.; Valastyan, Z.; Malandrinos, G.; Hadjiliadis, N.; Sovago, I. *Dalton Trans.* **2007**, 4040–4047.
(33) Mylonas, M.; Krezel, A.; Plakatouras, J. C.; Hadjiliadis, N.; Bal, W. *Bioinorg. Chem. Appl.* **2004**, *2*, 125–140.
(34) Kozłowski, H.; Kowalik-Jankowska, T.; Jezowska-Bojczuk, M. *Coord. Chem. Rev.* **2005**, *249*, 2323–2334.
(35) Rajkovic, S.; Kallay, C.; Serenyi, R.; Malandrinos, G.; Hadjiliadis, N.; Sanna, D.; Sovago, I. *Dalton Trans.* **2008**, 5059–5071.
(36) Mylonas, M.; Krezel, A.; Plakatouras, J. C.; Hadjiliadis, N.; Bal, W. *Bioinorg. Chem. Appl.* **2004**, *2*, 125–140.
(37) Rajkovic, S.; Kallay, C.; Serenyi, R.; Malandrinos, G.; Hadjiliadis, N.; Sanna, D.; Sovago, I. *Dalton Trans.* **2008**, 5059–5071.
(38) Boka, B.; Maryi, A.; Sovago, I.; Hadjiliadis, N. *J. Inorg. Biochem.* **2004**, *98*, 113–122.
(39) Jancso, A.; Paksi, Z.; Jakab, N.; Gyurcsik, B.; Rockenbauer, A.; Gajda, T. *Dalton Trans.* **2005**, 3187–3194.
(40) La Mendola, D.; Bonomo, R. P.; Caminati, S.; Giuseppe, N.; Emmi, S. S.; Hansson, O.; Maccarrone, G.; Pappalardo, G.; Pietropaolo, A.; Rizzarelli, E. *J. Inorg. Biochem.* **2009**, *103*, 195–204.

using a total volume of 1.6 cm^3. The purities and exact concentrations of the ligand solutions were determined by the Gran method.[41] The peptide concentration was 1×10^{-3} mol dm^{-3}, and the Zn^{2+}/Cu^{2+}/peptide ratio was 0.9:1:1 (this ratio was chosen to avoid excess Zn^{2+} in the solution, which led to hydrolysis of this ion). The pH-metric titrations were performed in 30:70 (v/v) dimethyl sulfoxide (DMSO)/water in 0.1 mol dm^{-3} KCl on a MOLSPIN pH-meter system using a normal Russel CMAW 711 semicombined electrode calibrated in proton concentrations using a 30:70 (v/v) DMSO/water solution of HCl. The calculated ionic product of DMSO/water was 14.511. The *HYPERQUAD 2006* program was used for stability constant calculations.[42,43] Standard deviations were computed by *HYPERQUAD 2006* and refer to random errors only. The constants for the hydrolytic Zn^{2+} species were used in these calculations.[44]

Mass Spectral Measurements. High-resolution mass spectra were obtained on a Bruker Q-FTMS spectrometer (Bruker Daltonik, Bremen, Germany), equipped with Apollo II electrospray ionization source with an ion funnel. The mass spectrometer was operated in the positive ion mode. The instrumental parameters were as follows: scan range, m/z 120−3500; dry gas, nitrogen; temperature, 170 °C; transfer time, 120 ps; the sample was in an aqueous solution of ammonium acetate (pH 6.8); collision voltage, −1,0 eV; 1:1:1 Zn^{2+}/Cu^{2+}/L metal-to-ligand ratio; $[Zn^{2+}]=10^{-4}$ M. The solution was infused at a flow rate of 3 μL/min. Before each run, the instrument was calibrated externally with a Tunemix mixture (Bruker Daltonik, Germany). The mass accuracy for the calibration was better than 5 ppm, enabling together with the true isotopic pattern (using SigmaFit) an unambiguous conformation of the elemental composition of the obtained complex.

CD Measurements. CD spectra were acquired on a Jasco J-815 spectropolarimeter at 298 K. A cell with a 0.1 cm path length was used for spectra recorded between 190 and 250 nm with sampling points every 1 nm. A 1 cm cell path length was used for data between 250 and 800 nm, with a 1 nm sampling interval. Four scans were collected for every sample with a scan speed of 100 nm/min and a bandwidth of 1 nm. Baseline spectra were subtracted from each spectrum, and data were smoothed with the Savitzky−Golay method.[45] Data were processed using the *Origin5.0* spread sheet/graph package. The direct CD measurements (θ, in millidegrees) were converted to mean residue molar ellipticity, using the relationship mean residue $\Delta\varepsilon = \theta/(33000c\times l\times$ number of residues).

NMR Experiments. NMR experiments were carried out at 14.1 or 11.8 T at controlled temperature (±0.1 K) on a Bruker Avance 600 or 500 MHz spectrometer equipped with a Silicon Graphics workstation. Suppression of the residual water signal was achieved either by presaturation or by excitation sculpting,[46] using a selective square pulse on water of 2 ms long. ^{1}H NMR resonance assignments were obtained by COSY, TOCSY, NOESY, and ROESY experiments. HSQC experiments were carried out with standard pulse sequences. Spectral processing was performed on a Silicon Graphics O2 workstation using the *XWINNMR 3.6* or *TOPSPIN 1.5* software. The diffusion coefficients were measured at 298 K by a PFG longitudinal eddy-current delay pulse sequence with bipolar gradients incorporating spoil gradients during both longitudinal storage periods.[47−49] The gradient strength was incremented (with an initial value of 0.86 G cm^{-1} and a step size of 2.65 G cm^{-1} for 2 ms), while the separations of the field gradients and the total echo time were kept constant. A series of 16 spectra, with a number of scans ranging from 16 to 32, were recorded in 2D mode for each measurement, with a recycle time of 10 s between scans. The diffusion values were calculated by regression analysis of the signal decay, leading to errors not larger than ±2−5%. The strength of the B_0 field gradient was calibrated by measuring the self-diffusion coefficient of the residual HDO signal in a 100% D_2O sample at 298 K.[50−52]

Molecular Dynamics (MD). Models for the various metal−peptide complexes were initially built through a simulated annealing procedure with the program *DYANA*,[53] using as restraints only the ones regarding metal coordination, i.e., distances of 0.2 nm between the metal and His imidazole Nδ atoms. Subsequently, energy minimization and MD simulation was performed on all of the systems, using the program *GROMACS*[54,55] with the OPLS force field[56] and maintaining the same restraints. The systems were minimized in vacuo and solvated in a parallelepiped box of SPC water with periodic boundary conditions, with a minimum distance between any atom of the peptide and the box edge of 1.5 nm. Cl^- counterions were added in order to neutralize the complex charge. The resulting systems were minimized again and brought to room temperature (298 K) through 3 runs of 10 ps each, in which the temperature was progressively raised. Then MD simulations at constant temperature ($T=298$ K) were performed. During the simulations, the peptide and solvent separately were weakly coupled to a temperature bath at the chosen temperature and to a pressure bath at 1 atm, with relaxation times $\tau_T = 0.1$ ps and $\tau_P = 0.5$ ps, respectively, using Berendsen's weak coupling algorithm;[57] bond lengths were constrained to equilibrium values using the SHAKE procedure,[58] with a geometric tolerance of 10^{-4}, and the time step was set to 1 fs. Nonbonded interactions were treated using a twin range method:[59] within a short-range cutoff of 0.8 nm, all interactions were determined at every time step, while longer range contributions within a cutoff of 1.4 nm were evaluated each time the pair list was generated.

Determination of SOD-like Activity. The in vitro SOD activities of the Cu^{2+} complexes were evaluated at 298 K, in samples containing $CuCl_2$ and peptide in the ratio 1:1 [$c_{Cu^{2+}}=(0-1)\times10^{-6}$ M] and $CuCl_2$, $ZnCl_2$, and peptide in the ratio 1:1:1 [$c_{Cu^{2+}}=(0-1)\times10^{-6}$ M] in a Tris−HCl buffer (25 mM, pH 7,4), with the metal ions and peptide being premixed.

The enzymatic activity was examined indirectly using the nitroblue tetrazolium (NBT) assay.[60]

(41) Gran, G. *Acta Chem. Scand.* **1950**, *4*, 559–577.
(42) Gans, P.; Sabatini, A.; Vacca, A. *J. Chem. Soc., Dalton Trans.* **1985**, 1195–1200.
(43) Gans, P.; Sabatini, A.; Vacca, A. *Talanta* **1996**, *43*, 1739–1753.
(44) Pettit, L. D.; Powell H. K. J. *The IUPAC Stability Constants Database*; IUPAC: London, 1992−2002.
(45) Savitzky, A.; Golay, M. *Anal. Chem.* **1964**, *36*, 1627–1639.
(46) Hwang, T. L.; Shaka, A. J. *J. Magn. Reson., Ser. A* **1995**, *112*, 275–279.
(47) Huber, J. G.; Moulis, J. M.; Gaillard, J. *Biochemistry* **1996**, *35*, 12705–12711.
(48) Gibbs, S. J.; Johnson, C. S. *J. Magn. Reson.* **1991**, *93*, 395–402.
(49) Dingley, A. J.; Mackay, J. P.; Chapman, B. E.; Morris, M. B.; Kuchel, P. W.; Hambly, B. D.; King, G. F. *J. Biomol. NMR* **1995**, *6*, 321–328.
(50) Johnson, C. S. *Prog. Nucl. Magn. Reson.* **1999**, *34*, 203–256.
(51) Callaghan, P. T.; Gros, M. A. L.; Pinder, D. N. *J. Chem. Phys.* **1893**, *79*, 6372–6381.
(52) Price, W. S. *Concepts Magn. Reson.* **1998**, *10*, 197–237.
(53) Güntert, P.; Mumenthaler, C.; Wüthrich, K. *J. Mol. Biol.* **1997**, *273*, 283–298.
(54) Lindahl, E.; Hess, B.; Van der Spoel, D. *J. Mol. Model.* **2001**, *7*, 306–317.
(55) Berendsen, H.; Van der Spoel, D.; Van Drunen, R. *Comput. Phys. Commun.* **1995**, *91*, 43–56.
(56) Jorgensen, W. L.; Tirado-Rives, J. *J. Am. Chem. Soc.* **1988**, *110*, 1657–1666.
(57) Berendsen, H.; Postma, J.; Gunsteren, W. F.; Di Nola, A.; Haak, J. *J. Chem. Phys.* **1984**, *81*, 3684–3690.
(58) Ryckaert, J.; Ciccotti, G.; Berendsen, H. *J. Comput. Phys.* **1977**, *23*, 327–341.
(59) Berendsen, H., Hermans, J., Eds. Polycrystal Book Service: Western Springs, PA, 1995; pp 18−22.
(60) Beauchamp, C.; Fridovich, I. *Anal. Biochem.* **1971**, *44*, 276–287.

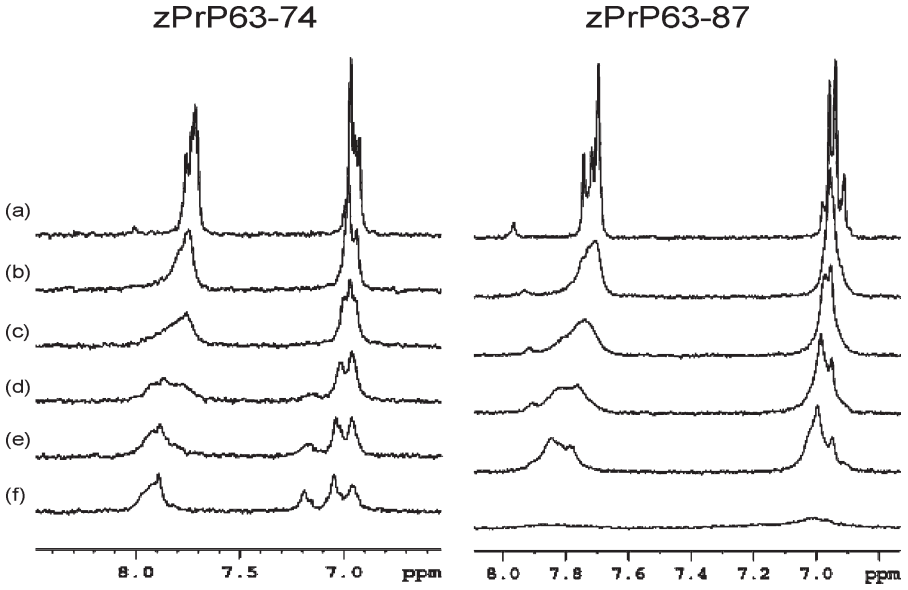

Figure 1. ^{1}H NMR spectra of (a) free peptides, (b) + 0.25 equiv of Zn^{2+}, (c) + 0.50 equiv of Zn^{2+}, (d) + 0.75 equiv of Zn^{2+}, (e) + 1.0 equiv of Zn^{2+}, and (f) + 2.0 equiv of Zn^{2+}. The peptides were 0.4 mM, pH 7.2, T = 298 K.

The superoxide anion was generated in situ by the xanthine−xanthine oxidase system and detected spectrophotometrically by monitoring the reduction of the NBT band at 560 nm. The assay contained (5×10^{-5} M) NBT, (10^{-4} M) xanthine, and an appropriate amount of xanthine oxidase to cause a change in absorbance at 560 nm of about $\Delta A_{560} = 0.025$ min^{-1}.

The reduction rate of NBT was measured in the presence as well as in the absence of the studied system. The control experiment was carried out in the presence of horseradish Cu, Zn−SOD [$(0-7)\times10^{-8}$ M]. The xanthine oxidase activity was monitored by the following of the urate production, spectrophotometrically at 298 nm, in order to exclude any inhibition induced by the Cu^{2+}−peptide complexes. The SOD-like activity was expressed by IC_{50} values, indicating the concentration of the SOD mimic, causing 50% inhibition of NBT reduction (with respect to the blank probe).

Results and Discussion

For the study of the Zn^{2+} and Cu^{2+} interaction with the zebrafish prion-related protein (zPrP-rel-2), three His-rich fragments, Ac-PVHTGHMGHIGH-NH_2 (zp-PrP63−74), Ac-PVHTGHMGHIGHTGHTGH-NH_2 (zp-PrP63−80), and Ac-PVHTGHMGHIGHTGHTGHTGSSGHG-NH_2 (zp-PrP63−87), were synthesized. The method of synthesis of the peptide was described previously.[29] In this study, potentiometric methods, UV−vis, CD, NMR spectroscopy, and mass spectrometry have been used.

Zn^{2+} and Cu^{2+} Homonuclear Complexes. All of the three investigated ligands (zp-PrP63−74, zp-PrP63−80, and zp-PrP63−87) effectively bind Cu^{2+} and Zn^{2+} ions.[29,31]

As previously described,[29] Cu^{2+} was bound to His imidazole N atoms at physiological pH; at higher pH, coordination to amide N atoms from peptide bonds was observed. Potentiometric data showed that also Zn^{2+} could effectively bind these ligands,[31] but its coordination mode was quite different from those observed for Cu^{2+}. In fact, Zn^{2+} was coordinated only by imidazole N atoms of His residues, and at pH > 7.5, hydroxo species were additionally formed.

In all of the analyzed systems, Zn^{2+} yielded similar variations on the NMR parameters (Figure 1). In particular, the presence of the metal ion caused large broadening and chemical shift variations especially on His resonances. The superimposition of His, Thr, and Gly spin systems and the large broadening did not allow one to assign unequivocally the NMR spectra such that the monitored effects were uniformly attributed to all of the His, Thr, and Gly present in the peptide sequence.

A metal titration was performed on zp-PrP63−74 in order to determine the affinity binding constants and the binding stoichiometry. Figure 1S in the Supporting Information shows the chemical shift variations measured at different Zn^{2+} amounts for some protons of zp-PrP63−74. The obtained results led us to obtain a K_d value in the 10 μM range and a stoichiometry of 1:1. On the contrary, no results could be obtained for the zp-PrP63−80 and zp-PrP63−87 systems because of the extensive Zn^{2+}-induced line broadening.

Figure 2 shows that Zn^{2+} ions most largely affect His and residues nearby (Thr, Gly, Met, and Ile). Moreover, Zn^{2+} binding to Nδ rather than to Nε is suggested by the larger shifts experienced by His Hε. These results were ratified by ^{1}H−^{13}C HSQC spectra, where, besides the ^{1}H NMR shifts already pointed out in Figure 2, extensive downfield ^{13}C NMR shifts (2.25 ppm) of His Hε were apparent (Figure 2S in the Supporting Information). zp-PrP63−87 and zp-PrP63−80 showed very similar variations of the NMR parameters (Figure 2), leading us to assume that the last seven residues and, in particular, His-86 did not play any key role in binding the metal. On the contrary, a different behavior was detected for zp-PrP63−74. Its chemical shift variations were almost twice as large as those measured on the other two systems (Figures 1 and 2), and also the Zn^{2+}-induced line broadenings were significantly different from those observed for the other peptides (Figure 1). While line broadening of zp-PrP63−74 reached a maximum in the presence of 0.75 equiv of Zn^{2+}, the NMR spectra of zp-PrP63−80 and zp-PrP63−87 were increasingly and continuously broadened by increases in the metal concentration up to 4.0 equiv of Zn^{2+}.

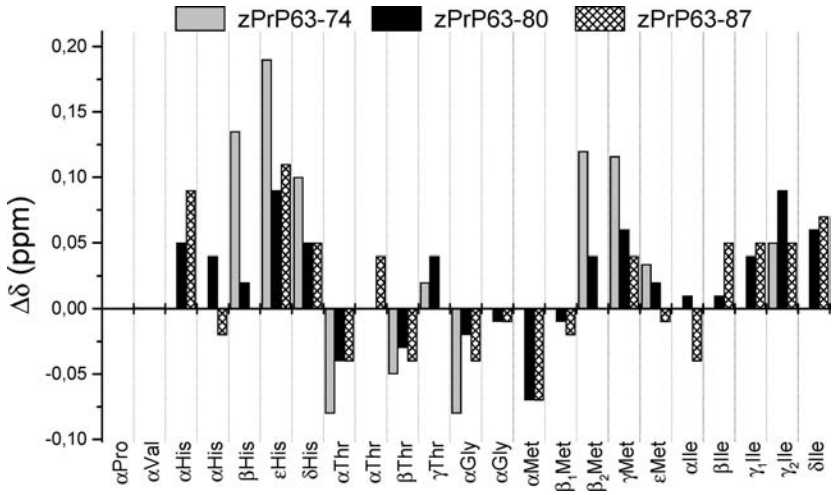

Figure 2. ^{1}H NMR shifts experienced by the three zebrafish peptides in the presence of Zn^{2+}. All of the peptides were 0.4 mM, pH 7.2, $T = 298$ K.

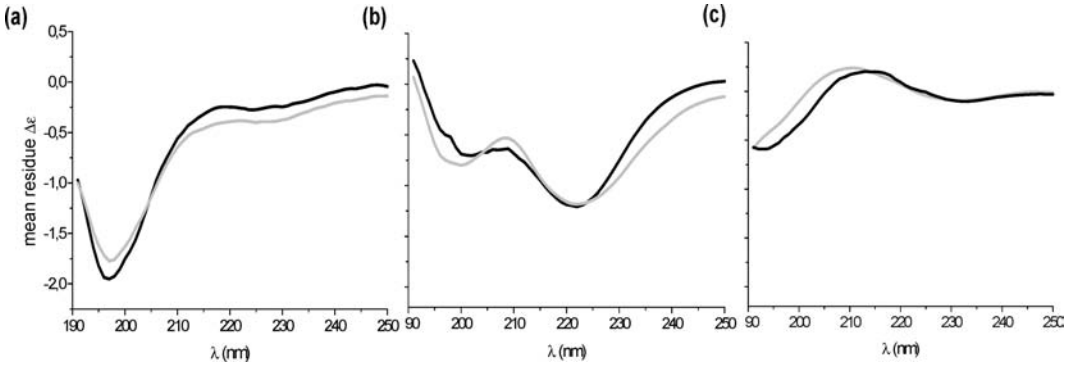

Figure 3. CD spectra of zp-PrP63−80 (gray) and zp-PrP63−87 (black) in the absence (a) and in the presence of 1 equiv of Cu^{2+} (b) or 1 equiv of Zn^{2+} (c). All of the peptides were 0.1 mM, pH 7.2, $T = 298$ K.

Because of the diamagnetic nature of Zn^{2+}, the observed line broadening might be explained either by the occurrence of an intermediate exchange regime or by aggregation phenomena. The diffusion coefficient experiments were performed in the absence and in the presence of increasing Zn^{2+} amounts. All of the measured diffusion coefficients (calculated by diffusion-order NMR spectroscopy) were very similar (data not shown), thus excluding the formation of aggregates. The occurrence of an intermediate (in the NMR time scale) exchange regime between two or more states was therefore considered. The observed differences were attributed to the existence of different equilibria in solution. In the case of zp-PrP63−74, the effects shown in Figure 1 are consistent with chemical exchange between the free and metal-bound form (the maximum broadening is expected when the bound and free forms are equally populated), whereas in the cases of zp-PrP63−87 and zp-PrP63−80, chemical exchange between different bound states (1:1 and 2:1) was assumed because, as was already reported, both fragments can cooperatively bind Zn^{2+}.[31]

In particular, mass spectra showed the existence of three different species belonging to (1) free peptides (L), (2) ZnL, and (3) Zn_2L.[31] Also for copper, we observed two different ESI-MS signals arising from both CuL and Cu_2L complexes (data not shown). The occurrence of the Cu_2L species was the result of Cu^{2+} cooperative binding where coordination of the first Cu^{2+} ion promoted the binding of the second metal ion.

Far-UV CD was used to monitor any structural rearrangements of the zebrafish systems upon Cu^{2+} and Zn^{2+} addition. The CD spectra of all of the peptides in the absence of metals showed a strong intense negative band at 198 nm, characteristic of random-coil conformation (Figure 3A).

The addition of Cu^{2+} significantly changed the CD spectra. The intensity of the band at 198 nm was progressively decreasing and the intensity of the new negative band at 222 nm was progressively increasing as the Cu^{2+} concentration was increased, suggesting a Cu^{2+}-induced profound structuring of the main chain (Figure 3B).

Also, the binding of Zn^{2+} to zp-PrP63−80 and zp-PrP63−87 affected the CD spectra such that a new weak positive band appeared at 209 nm, while the "random-coil" band was strongly reduced (Figure 3C).

The large modifications observed in the CD spectra indicate that Cu^{2+} and/or Zn^{2+} binding leads to strong structural rearrangements of the peptide main chain and that the conformational changes strongly depend on the different geometries (tetragonal vs tetrahedral) of the metal coordination spheres.

The copper and zinc binding abilities of zp-PrP63−80 and zp-PrP63−87 were also compared by analysis of the competition plot reported in Figure 4. Such data showed that Cu^{2+} binds to zp-PrP63−80 and zp-PrP63−87 with

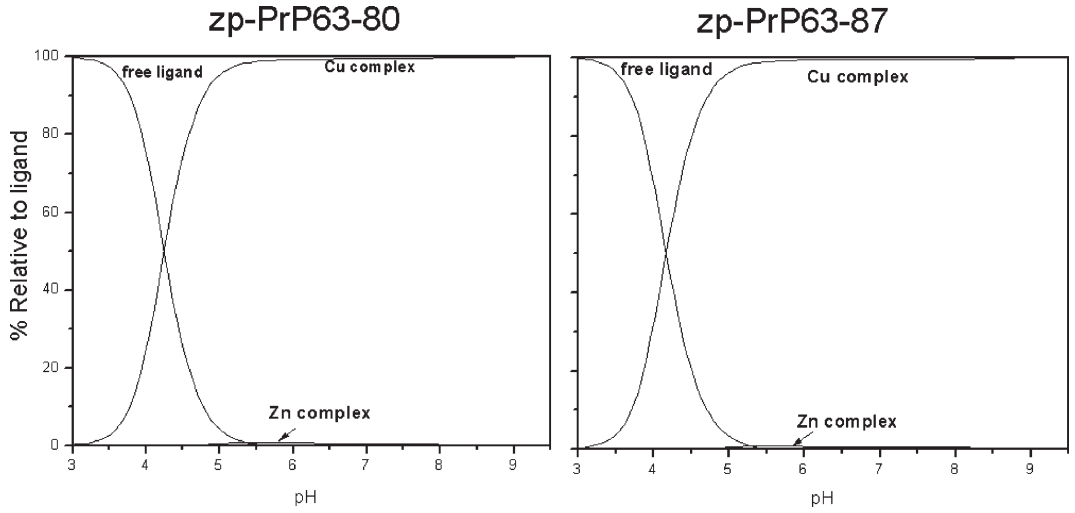

Figure 4. Competition plots showing the affinity of Cu^{2+} and Zn^{2+} ions to zp-PrP63−80 and zp-PrP63−87 protein fragments. $c_{Zn^{2+}} = 0.001$ M; 1:1:1 Zn/Cu/L.

much larger affinity than Zn^{2+} does. CD spectra were also performed to additionally confirm the competition between the two metal ions. CD spectra recorded in the 800−350 nm wavelength region are usually used to extrapolate information on the copper coordination sphere. CD spectra of zp-PrP63−80 and zp-PrP63−87 Cu^{2+} complexes before and after the addition of Zn^{2+} showed no differences (data not shown), supporting the fact that binding of Zn^{2+} did not change the copper binding mode and that Cu^{2+} was not replaced by Zn^{2+}.

Structural Model of Zn_2-zPrP63−87 and Cu_2-zPrP63−87. NOESY experiments were performed on samples containing Zn^{2+}: unfortunately, any "not trivial" correlation was found, indicating that the metal binding induces no particular secondary structure (α helix, β sheet) on the peptide main chain.

The large structuring differences induced by Cu^{2+} and Zn^{2+}, suggested by CD data, were analyzed by MD simulations. The investigated systems were metal complexes of the zp-PrP63−87 fragment, with two metal ions bound in a multihistidine mode, to Nδ imidazole atoms of His-65, His-68, and His-71 (the first) and to His-74, His-77, and His-80 (the second), as found by these and previous investigations.[29] We did not take into account the possible involvement of His-86, in light of the similar NMR and CD behavior of the zp-PrP63−87 and zp-PrP63−80 peptides. In order to compare the effects of the different coordination properties of Cu^{2+} and Zn^{2+} on the peptide conformation, we considered two cases, corresponding to the Zn_2-zp-P63−87 and Cu_2-zp-PpP63−87 complexes. Both systems were simulated for 20 ns. The global backbone root-mean-square deviation (rmsd) with respect to the initial conformation was monitored during the whole MD trajectory (Figure 3S in the Supporting Information). The rmsd values were stabilized to 0.6−0.8 nm after 10 ns, suggesting system equilibration. Therefore, only the last 10 ns were further analyzed. Figure 4S in the Supporting Information shows the secondary structure along the last 10 ns of the MD trajectories of the two complexes, and Table 1 summarizes the secondary structure content for the two simulations.

In all investigated cases, peptide does not assume a definite secondary structure, with the exception of a few helical segments, as is also shown by the high percentage of random coil. The main structural elements present in all of the simulated systems are bends and turns whose secondary structure content is about 40% for both complexes. Interestingly, the bends and turns percentages in the two complexes are roughly inverted: 10.7% of bends and 25.9% of turns for the Zn^{2+} complex and 25.3% of bends and 14.0% of turns for the Cu^{2+} complex. Other peculiar differences can be observed in the region of the two metal binding sites (in particular, residues 65−68, i.e., residues 3−6 in the numbering used in Figure 4S in the Supporting Information) where the Zn−Zn complex displays more definite helical elements than the other complex. Parts A and B of Figure 5 report 20 snapshots of the last 10 ns of the MD trajectories for Zn_2-zp-PrP63−87 and Cu_2-zp-PrP63−87, respectively.

Table 1. Secondary Structure Content (Number of Residues and Percentage), Averaged over the Last 10 ns, for the Two Simulations[a]

	coil	β sheet	β bridge	bend	turn	α helix	3 helix	tot. helix
				ZnZn				
average	8.12	0.26	3.11	2.88	6.99	0.62	3.01	3.63
%	30.09	0.98	11.51	10.68	25.90	2.30	11.14	13.44
				CuCu				
average	13.39	0.00	0.91	6.84	3.79	0.00	0.07	0.07
%	49.59	0.00	3.37	25.34	14.02	0.00	0.28	0.28

[a] "tot. helix" is the sum of the two preceding columns.

The overall structures of the Zn_2-zp-PrP63−87 system are more compact and better defined than those of the Cu_2-zp-PrP63−87 complex. Also, the metal binding sites are better resolved and include more defined structuring elements. These data support the hypothesis of a local structuring induced by metal coordination and are dependent on the geometry of the coordination sphere, in agreement with the results of CD measurements.

Zn^{2+} and Cu^{2+} Heteronuclear Complexes. As reported here and in previous investigations, zp-PrP63−74, zp-PrP63−80, and zp-PrP63−87 effectively bind Cu^{2+} and

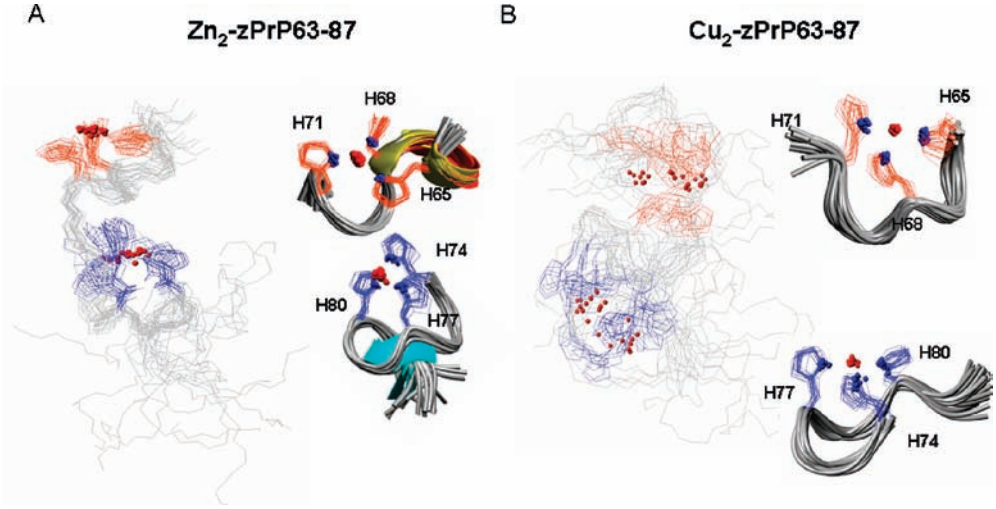

Figure 5. A total of 20 snapshots from the last 10 ns of the MD simulations, showing the overall structure and the two metal binding sites of the metal complexes with the zp-PrP63−87 system. (A) Zn_2-zp-PrP63−87. rmsd value (taken on residues 65−81) 0.117 ± 0.042 nm for the backbone atoms and 0.142 ± 0.045 nm for the heavy atoms; rmsd value (taken on residues 65−72) 0.043 ± 0.012 nm for the backbone atoms and 0.080 ± 0.018 nm for the heavy atoms;. rmsd value (taken on residues 74−81) 0.059 ± 0.018 nm for the backbone atoms and 0.077 ± 0.020 nm for the heavy atoms. (B) Cu_2-zp-PrP63−87. rmsd value (taken on residues 65−81) 0.312 ± 0.174 nm for the backbone atoms and 0.350 ± 0.187 nm for the heavy atoms; rmsd value (taken on residues 65−72) 0.095 ± 0.044 nm for the backbone atoms and 0.136 ± 0.046 nm for the heavy atoms;. rmsd value (taken on residues 74−81) 0.067 ± 0.023 nm for the backbone atoms and 0.087 ± 0.028 nm for the heavy atoms;

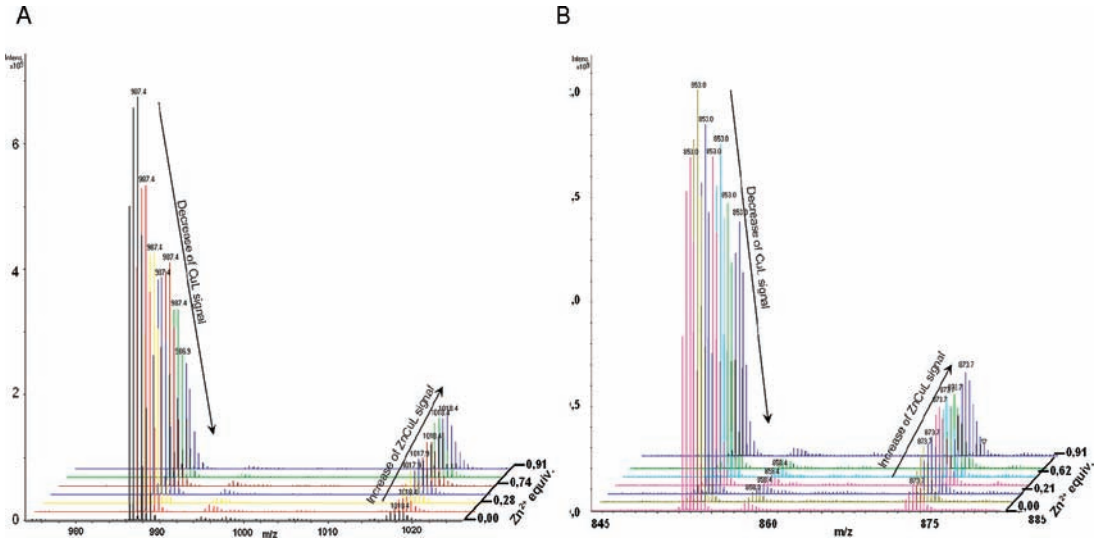

Figure 6. (A) ESI-MS spectra of a system containing Cu^{2+} and zp-PrP63−80 in the stoichiometry 1:1 Cu/L after titration with Zn^{2+} ions until the stoichiometry 0.98:1:1 Zn/Cu/L is reached. $c_{zp\text{-}PrP63-80(initial)} = 0.3$ mM; $c_{Cu^{2+}(initial)} = 0.29$ mM. (B) ESI-MS spectra of a system containing Cu^{2+} and zp-PrP63−87 in the stoichiometry 1:1 Cu/L after titration with Zn^{2+} ions until the stoichiometry 0.98:1:1 Zn/Cu/L is reached. $c_{zp\text{-}PrP63-80(initial)} = 0.26$ mM; $c_{Cu^{2+}(initial)} = 0.25$ mM.

Zn^{2+}. The presence of six or seven His makes the last two systems potential candidates to bind both metal ions simultaneously, yielding to the formation of heteronuclear Zn−Cu complexes.

In order to verify the presence of heteronuclear complexes in solution, ESI-MS spectra were performed. A series of mass spectra were recorded by adding different amounts of Zn^{2+} to equimolar Cu^{2+}-zp-PrP63−80 (Figure 6A) and Cu^{2+}-zpPrP63−87 (Figure 6B) solutions. The titrations showed that, by an increase in the zinc concentration, the intensity of the CuL signal decreased, while that of the Zn−CuL complex increased (L = zp-PrP63−80 or zp-PrP63−87). An enlarged view of Figure 6 (Figure 5S in the Supporting Information) better evidences how the signals at about m/z 1018 and 874 respectively for zpPrP63−80 and zpPrP63−87 increased after the Zn^{2+} addition, strongly suggesting the occurrence of heteronuclear complexes. The formation of heteronuclear complexes is summarized by the following reactions:

$$[Cu(zp\text{-}PrP63-80)]^{2+} + Zn^{2+} \rightarrow Zn[Cu(zp\text{-}PrP63-80)H_{-2}]^{2+} + 2H^{+}$$

$$[Cu(zp\text{-}PrP63-87)H]^{3+} + Zn^{2+} \rightarrow Zn[Cu(zp\text{-}PrP63-87)H_{-2}]^{3+} + 2H^{+}$$

For both peptides, the signal of the Cu_2L complex almost overlaps the ZnCuL signal. However, the

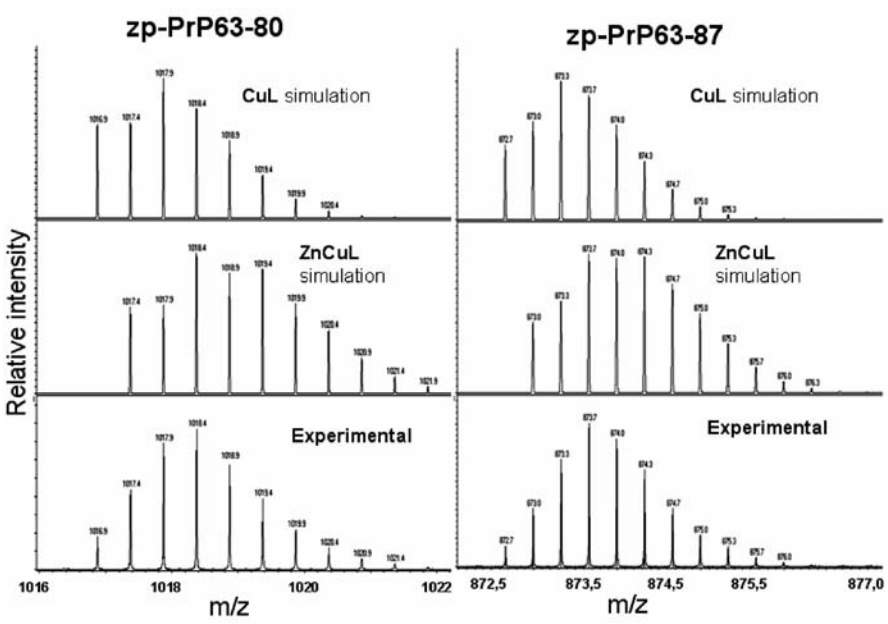

Figure 7. Simulation and ESI-MS experimental spectra of Cu_2L and ZnCuL complexes where L = zp-PrP63−80 and zp-PrP63−87. $c_{\text{zp-PrP63-80}}$ = 0.25 mM, $c_{Cu^{2+}}$ = 0.246 mM, $c_{Zn^{2+}}$ = 0.212 mM and $c_{\text{zp-PrP63-87}}$ = 0.24 mM, $c_{Cu^{2+}}$ = 0.234 mM, $c_{Zn^{2+}}$ = 0.21 mM.

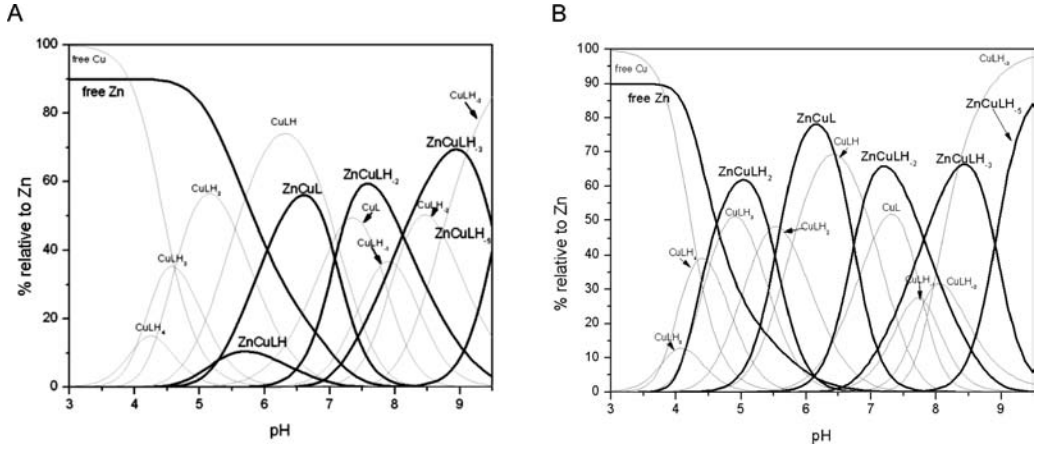

Figure 8. (A) Overlapping of species distribution profiles for Zn−Cu-zp-PrP63−80 complexes (0.9:1:1), $c_{Zn^{2+}}$ = 0.0009 M (dark line), and for 1:1 Cu-zp-PrP63−80 (gray line). (B) Overlapping of species distribution profiles for Zn−Cu-zp-PrP63−87 complexes (0.9:1:1), $c_{Zn^{2+}}$ = 0.0009 M (dark line), and for 1:1 Cu-zp-PrP63−87 (gray line).

formation of the ZnCuL complexes was confirmed by analysis of the isotopic distribution of the signals and by comparison of the experimental spectra with the simulated ones (Figure 7).

The occurrence of heteronuclear species for both zp-PrP63−80 and zp-PrP63−87 urged us to characterize it by using potetiometric, NMR, and CD techniques.

Potentiometric results are shown in Table 1S in the Supporting Information and in Figure 8. The distribution diagrams reported in Figure 8 show the superimposition between the Cu and ZnCu complex species. The fact that Zn^{2+} is bound with much lower affinity than Cu^{2+} enabled us to assume that Zn^{2+} did not influence the copper coordination mode. Using this assumption, we directly compared the binary (Cu/L) and ternary (Zn/Cu/L) systems. For zp-PrP63−80 (Figure 8A), only Cu^{2+} complexes were present at pH <4.5: the $CuLH_4$ and $CuLH_3$ forms corresponded to Cu^{2+} bound to two and three His imidazole rings, respectively. Above pH 4.5, the first heteronuclear complex (Zn−CuLH) was formed. It corresponded to the $CuLH_2$ and CuLH forms observed in the Cu^{2+} system. The comparison of these two species indicates that a Cu^{2+} ion was bound to four imidazole rings from His residues ($4N_{im}$), whereas the binding of Zn^{2+} resulted in the deprotonation of one additional His only, which results in the Zn−CuLH species.

At pH 6.5, the Zn−CuL complex was formed (Figure 9A), which corresponded to the CuHL species, observed in the system containing only Cu^{2+}. The comparison between the ternary (Zn^{2+} and Cu^{2+}) and the Cu^{2+}-containing systems showed that Cu^{2+} was bound to four imidazole rings from His residues ($4N_{im}$), whereas Zn^{2+} was bound to two imidazole groups and the two remaining coordination sites were probably filled by water molecules {$2N_{im}$ and $2H_2O$}. At pH >7, in the Cu^{2+}-containing systems, the CuL, $CuLH_{-1}$, $CuLH_{-2}$,

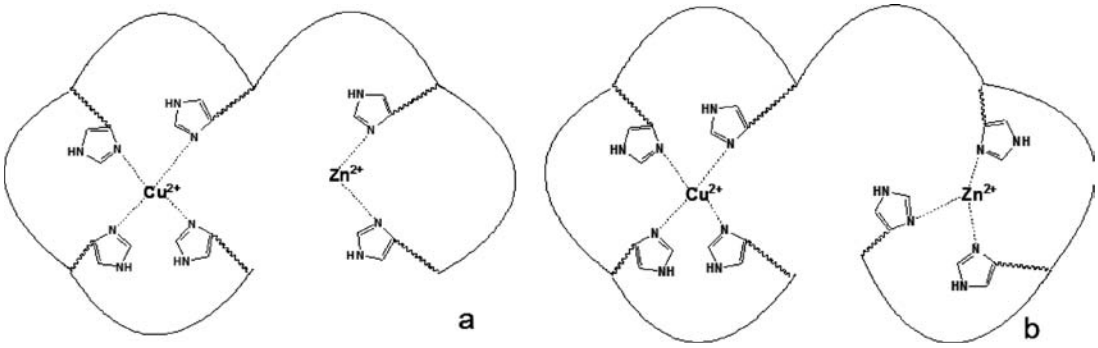

Figure 9. Proposed structures of isomers of the CuL complex where L is the (a) zp-PrP63−80 and (b) zp-PrP63−87 fragment.

and $CuLH_{-3}$ species were formed. In these complexes, the Cu^{2+} donor atoms gradually changed from imidazole to amide N atoms derived from the peptide bonds until the $\{N_{im}$ and $3N^-\}$ coordination mode was achieved. In the same pH range, in the ternary (Zn^{2+} and Cu^{2+}) system, $ZnCuLH_{-2}$, $ZnCuLH_{-3}$, and $ZnCuLH_{-5}$ complexes were formed. The $ZnCuLH_{-2}$ complex was the main species, whereas in the Cu^{2+}-containing system, the CuL and $CuLH_{-1}$ species prevailed. This fact indicated that the first observed deprotonation from the ZnCuL to $ZnCuLH_{-2}$ species corresponded to changes in the Cu^{2+} coordination mode from ($4N_{im}$) to ($3N_{im}$, N^-) and in the Zn^{2+} mode from ($2N_{im}$, $2H_2O$) to ($2N_{im}$, H_2O, OH^-). The comparison of Cu^{2+}-containing and Zn^{2+}- and Cu^{2+}-containing systems clearly showed that in the case of the $ZnCuLH_{-5}$ complex (which corresponds to $CuLH_{-3}$ species present in binary systems) the coordination mode of Cu^{2+} is (N_{im}, $3N^-$). The two additional deprotonations arose from the water molecules bound to Zn^{2+} with the formation of the $ZnCuLH_{-5}$ (or rather $ZnCuLH_{-3}(OH^-)_2$) complex.

Figure 8B shows the superimposition of the species distribution profiles of Zn−Cu-zp-PrP63−87 complexes. The formation of the heteronuclear Cu^{2+} and Zn^{2+} complex was very similar to that of the Zn−Cu-zp-PrP63−80 system described above. Very interesting conclusions were obtained after the comparison of the stability constants of the Zn−CuL species (where L is zp-PrP63−80 or zp-PrP63−87; Table 1S in the Supporting Information and Figure 9A,B). The compex with the additional TGSSGHG tail was more stable and the stability constants differed by 1.8 logarithmic unit, suggesting the possible involvement of His-86 with a consequent stabilizing effect.

NMR experiments were also performed on zp-PrP63−80 and zp-PrP63−87 samples in the presence of both Cu^{2+} and Zn^{2+} in order to characterize the heteronuclear species already detected by mass spectrometry. NMR alone may not be revealing enough for the exclusive formation of the ZnCu species because the formation of separate Zn^{2+} and Cu^{2+} complexes in solution cannot be excluded a priori. However, the different effects of the metals, i.e., Zn^{2+}-induced chemical shifts and Cu^{2+}-determined impressive line broadenings, could be used to localize the two binding sites. Figure 10 shows ^1H NMR spectra of zp-PrP63−87 in the presence of Cu^{2+} and Zn^{2+}. As is usually found,[29] the addition of Cu^{2+} yields a dramatic line broadening of His signals, with the His aromatic protons being completely washed out upon the addition of 0.5 equiv of Cu^{2+} (Figure 10f). The successive additions of Zn^{2+} (0.25, 0.50, and 0.75 equiv) resumed the appearance of His aromatic signals, which, although very broad, were shifted with respect to the free signals. These findings strongly support the involvement of the His imidazole ring in both Cu^{2+} and Zn^{2+} binding.

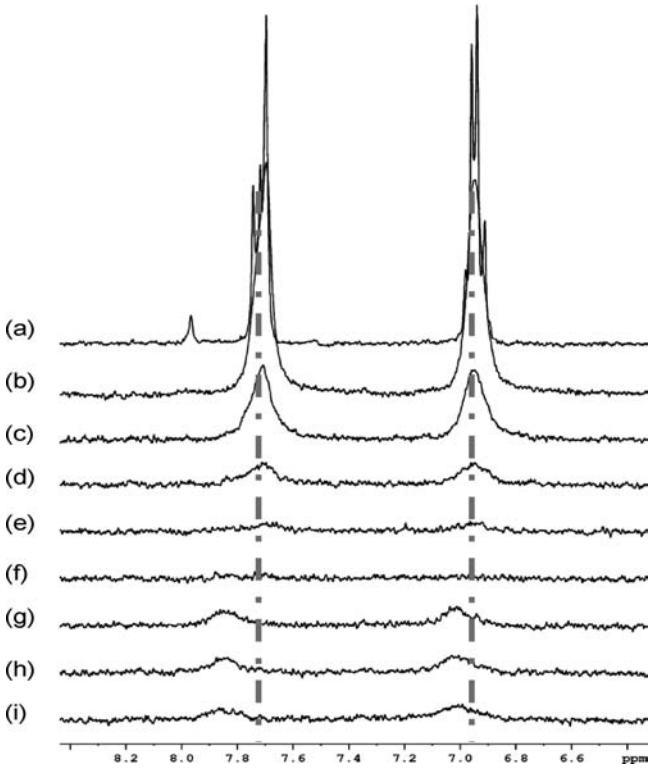

Figure 10. ^1H NMR spectra of (a) free zp-PrP63−87, (b) + 0.10 equiv of Cu^{2+}, (c) + 0.20 equiv of Cu^{2+}, (d) + 0.30 equiv of Cu^{2+}, (e) + 0.40 equiv of Cu^{2+}, (f) + 0.50 equiv of Cu^{2+}, (g) + 0.50 equiv of Cu^{2+} + 0.25 equiv of Zn^{2+}, (h) + 0.50 equiv of Cu^{2+} + 0.50 equiv of Zn^{2+}, (i) + 0.50 equiv of Cu^{2+} + 0.75 equiv of Zn^{2+}. The peptides were 0.4 mM, pH 7.2, $T = 298$ K.

The simultaneous effects of the two metal ions were also monitored by analyzing 2D $^1H-^1H$ TOCSY maps in order to better characterize the two metal binding sites. Figure 11 reports the zp-PrP63−87 spectra recorded in the presence of 0.75 equiv of Zn^{2+} (black contours) and 0.75 equiv of Cu^{2+} (blue contours) and in the presence of both 0.75 equiv of Cu^{2+} and 0.75 equiv of Zn^{2+} (magenta contours).

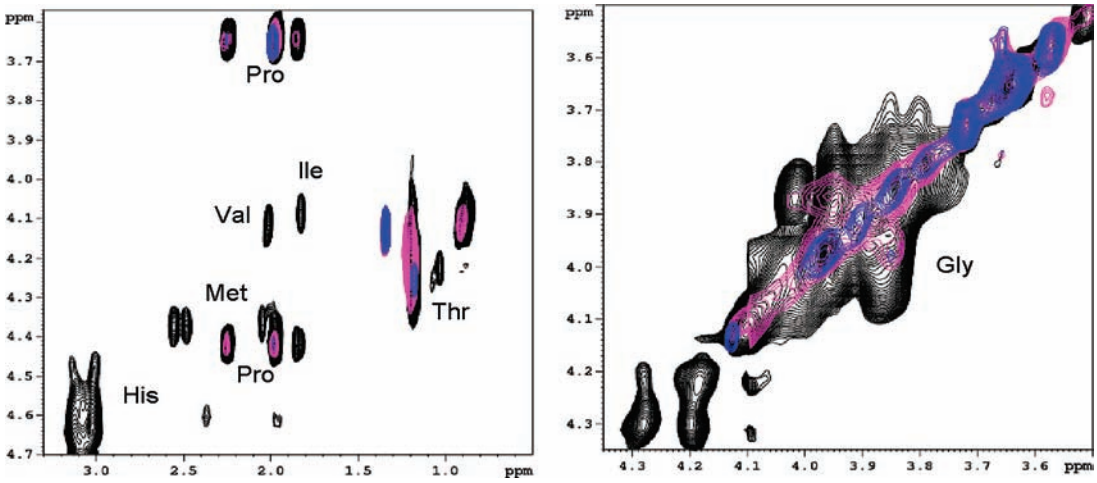

Figure 11. Selected regions of $^1H-^1H$ TOCSY spectra of zp-PrP63−80, 0.4 mM, pH 7.2, in the presence of 0.75 equiv of Zn^{2+} (black), 0.75 equiv of Cu^{2+} (blue), and 0.75 equiv of Zn^{2+} and 0.75 equiv of Cu^{2+} (magenta).

The magenta and blue contours are notably less intense than the black one because of the presence of the paramagnetic Cu^{2+}, which strongly affects the proton transverse relaxation rates, inducing a dramatic line broadening. However, the comparison between the magenta and black contours shows that the His, Met, Val, and Ile correlations, detectable in the presence of Zn^{2+}, disappear in the spectra recorded in the presence of Cu^{2+}; on the contrary, Thr and Gly correlations, although weak, are still detectable in the sample containing both metal ions but not in the one containing only Cu^{2+}. Because Met, Val, and Ile are all in the N-terminal part, such findings are consistent with Cu^{2+} binding to the first four or three His side chains (His-65, His-68, and His-71) while the last two or three His side chains (His-74, His-77, and His-80) are likely to be bound to Zn^{2+}.

CD experiments were also performed on peptide solutions containing both Cu^{2+} and Zn^{2+}. The obtained spectrum (Figure 6S in the Supporting Information) was then compared to different linear combinations of the spectra recorded in the presence of only Cu^{2+} or Zn^{2+}. None of the combined spectra matched the experimental one, strongly suggesting the presence of a heteronuclear species in solutions giving its own CD absorptions.

SOD-like Activity. The SOD activities (given as IC_{50} values, that is, as the concentrations of complexes required to attain 50% inhibition of NBT reduction) of all of the copper-containing complexes are listed in Table 2, together with the IC_{50} values of other biologically important ligands (at pH 7.4), representing the best SOD mimics reported so far (note that the smaller the IC_{50} value, the higher the SOD activity).

The speciation is considered to be an important issue for interpretation of the in vitro SOD-like activity of all four complexes. Equilibrium studies of all of these systems confirmed that both Cu^{2+} and Zn^{2+} are almost completely bound at pH 7.4. The metal ions are bound to both histidyl imidazole side chains and amide groups. It has been shown[30] that amide coordination has a negative effect on the SOD activity.

Both Cu^{2+} and $Zn^{2+}-Cu^{2+}$ complexes exhibit catalytic activity toward the dismutation of superoxide anions. All of the IC_{50} values are considerably higher than those of the native SOD (IC_{50} value of 0.0081 μM) but comparable to the activity of the Ac-PHGGGWGQ-NH_2 fragment from the human prion octarepeat region.[30]

Table 2. IC_{50} (μM) Values of Reports on SOD-like Activity of Copper(II) Complexes

species	IC_{50} (μM)	ref
Cu-zp-PrP63−80	0.615	this work[29]
Cu−Zn-zp-PrP63−80	0.601	this work
Cu-zp-PrP63−87	0.604	this work[29]
Cu−Zn-zp-PrP63−87	0.592	this work
$CuCl_2$	0.998	this work
bovine SOD	0.0081	this work
human PrP: 1:1 Cu^{2+}/1Oct[a]	0.492	30
human PrP: 1:1 Cu^{2+}/4Oct[b]	0.175	30
$[Cu_2(bdpi)(CH_3CN)_2](ClO_4)_3\cdot CH_3CN\cdot H_2O$[c]	0.32	61
$[CuZn(bdpi)(CH_3CN)_2](ClO_4)_3\cdot 2CH_3CN$[c]	0.24	61
$[LCu_2(im)](ClO_4)_3(H_2O)_{2.5}(CH_3CN)_{0.5}$[d]	0.36	62
(Cu^{2+}−im−Cu^{2+}) cryptand[e]	0.5	63
(Cu^{2+}−im−Zn^{2+}) cryptand[e]	0.5	63
1:1 Cu^{2+}/ HGDHMHNHDTK[f]	0.31	64

[a] Ac-PHGGGWGQ-NH2. [b] Ac-(PHGGGWGQ)4-NH2. [c] Hbdpi = 4,5-bis[(di-2-pyridylmethyl)aminomethyl]imidazole. [d] LL′3,6,9,17,20,23-hexaza-6,20-bis(2-hydroxyethyl)tricyclo[23.3.1.1.11,15]triaconta-1(29),11(30),12,14,25,27-hexene, imL′imidazole. [e] Cryptand L′1,4,12,15,18,26,31,39-octaazapentacyclo[13.13.13.1.1.1]tetratetracontane-6,8,10,20,22,24,33,35,37-nonene. [f] (pH 8.2) (SOD fragment isolated from Hemophilus ducreyi).

For both zp-PrP63−80 and zp-PrP63−87, the SOD-like activity improves only slightly when Zn^{2+} is added to the Cu^{2+}−peptide system. The improvement of the SOD-like activity after the addition of Zn^{2+} ions is relatively lower compared to that found earlier for ternary $Cu^{2+}-Zn^{2+}$ complexes (Table 2).[61]

Conclusion

An important issue about the interactions between PrP derived from fishes and metal ions is the fact that the protein

(61) Ohtsu, H.; Shimazaki, Y.; Odani, A.; Yamauchi, O.; Mori, W.; Itoh, S.; Fukuzumi, S. *J. Am. Chem. Soc.* **2000**, *122*, 5733–5741.
(62) Yang, D.-X.; Li, S.-A.; Li, D.-F.; Chen, M.; Huang, J.; Tang, W.-X. *Polyhedron* **2003**, *22*, 925–932.
(63) Pierre, J.-L.; Chautemps, P.; Refaif, S.; Beguin, C.; El Marzouki, A.; Serratrice, G.; Saint-Aman, E.; Rey, P. *J. Am. Chem. Soc.* **1995**, *117*, 1965–1973.
(64) Paksi, Z.; Jancsó, A.; Pacello, F.; Nagy, N.; Battistoni, A.; Gajda, T. *J. Inorg. Biochem.* **2008**, *102*, 1700–1710.

can effectively bind Cu^{2+} and Zn^{2+} ions. Full characterization of the complex formation at physiological pH was possible by correlation of the experimental data obtained from NMR, ESI-MS, potentiometric, and CD methods. MS spectra confirmed the formation of ternary complexes and showed the stoichiometry of the species. Potentiometric titrations allowed us to determine the stability constants and pH-dependent profile of the investigated systems, and NMR allowed us to identify the binding donor atoms.

These and previous findings strongly support copper and zinc binding to the N-terminal region of zebrafish PrP-rel2 protein. The polyhistidine sequence encompassing residues 63−87 allows the formation of mono- and binuclear (homo- and heteronuclear) species. Both metals were shown to bind cooperatively to 63−87 fragments; their interaction yielded very strong structural rearrangements of the backbone main chain strongly dependent on the metal ion type. The comparison between zp-PrP63−87 and zp-PrP63−80 complexes indicated that the metal interaction is not affected by the additional presence of the C-terminal tail, revealing a minor role for His-86.

The comparison of the affinities of copper and zinc toward the PrP-rel peptide fragments showed that the binding of copper is much more effective than the binding of zinc. This finding, together with the NMR data, clearly shows that the zp-PrP63−80 and zp-PrP63−87 fragments can bind Cu^{2+} by His donors $\{4N_{im}\}$ and at higher pH by His and amide N atom $\{N_{im}, 3N^{-}\}$ donors, whereas Zn^{2+} is bound by four imidazole groups $\{4N_{im}\}$. These His-rich domains can effectively bind Cu^{2+} and Zn^{2+} in a heteronuclear complex at physiological pH using His imidazole N donors. Ternary complexes of Cu^{2+} and Zn^{2+} with three peptide sequences derived from a prion-related protein of zebrafish can act as SOD−mimic systems although their activity is not much improved by the presence of Zn^{2+} ions.

Acknowledgment. We acknowledge MIUR (FIRB RBNE03PX83_003) for financial support and CIRMMP (Consorzio Interuniversitario Risonanze Magnetiche di Metalloproteine Paramagnetiche) for providing access to CERM instrumentations. This work was supported by the Polish Ministry of Science and Higher Education (Project 1 T09A 008 30).

Supporting Information Available: ^{1}H NMR chemical shift variations of zp-PrP63−74 (Figure 1S), ^{13}C NMR shifts experienced by zPrP63−87 (Figure 2S), backbone rmsd values during the whole 20 ns trajectories of Zn_2-zPrP63−87 and Cu_2-zPrP63−87 MD simulations (Figure 3S), secondary structure plots for the Zn,Zn (A), Cu,Cu (B) simulations (Figure 4S), overlapping of ESI-MS spectra of the Cu:(zp-PrP73−80) and Cu:(zp-PrP73−87) (stoichiometry 1:1) systems (Figure 5S), CD spectra of and zp-PrP63−87 (black) in the presence of both 1 equiv of Cu^{2+} and 1 equiv of Zn^{2+} (Figure 6S), and potentiometric data for H^{+}, Cu^{2+}, and Zn^{2+} Cu^{2+} complexes (Table 1S). This material is available free of charge via the Internet at http://pubs.acs.org.